A Multi-Model Assessment of Evolving Forced Changes in Northern Hemisphere Modes of Atmospheric Circulation Variability and the Role of the Tropical Pacific

Nicola Maher,[1,2*], Clara Deser[3] and John P. O'Brien[4]

[1]Research School of Earth Sciences, Australian National University, Canberra, ACT, Australia.
[2]ARC Centre of Excellence for Weather of the 21st Century, Australian National University, Canberra, ACT, Australia.
[3]Climate and Global Dynamics Laboratory, National Center for Atmospheric Research, Boulder, Colorado, USA.
[4]Heising-Simons Foundation, Los Altos, California, USA.

*Corresponding author(s). E-mail(s): nicola.maher@anu.edu.au;

Abstract

Understanding how modes of climate variability will change in a warming world is essential for improving regional climate projections. Using eight single model initial-condition large ensembles (SMILEs), we examine projected changes in the leading Northern Hemisphere modes of wintertime atmospheric circulation variability: the Pacific North American (PNA) pattern, the North Pacific Oscillation (NPO), the East Pacific Pattern (EPP), and the North Atlantic Oscillation (NAO), and their influence on precipitation. By applying a snapshot empirical orthogonal function (SEOF) analysis to the 500hPa geopotential height field in each SMILE, we are able to characterise how patterns, amplitudes, and impacts of each mode are projected to evolve over the next century. While most of the SMILEs generally capture the observed modes of variability, we find substantial disagreement in their projections of the NPO and NAO. The PNA response is more robust across models and is associated with a consistent intensification of the Aleutian low variability, which has implications for the volatility of future precipitation patterns over the United States. Both the PNA and NPO projections become more consistent between models when influences from the tropical Pacific are removed, highlighting that inter-model differences in projections of the

El Niño Southern Oscillation can confound projections of extra-tropical modes of variability. In contrast, NAO projections remain model-dependent even when tropical Pacific influences are removed. The EPP emerges as an increasingly important mode for Californian precipitation in the future, with its influence obscured by the tropical Pacific. Overall, our results demonstrate that there is still much research to be done to better understand projected changes in modes of climate variability and their impacts, given the large inter-model spread.

Keywords: ENSO, modes of variability, atmospheric circulation teleconnections, large ensemble, snapshot EOF

1 Introduction

Understanding our climate requires information about both the mean state and the variability around it. A key expression of such variability in the climate system is through preferred patterns or "modes" that fluctuate between negative and positive phases such as the North Atlantic Oscillation (NAO) and the El Niño Southern Oscillation (ENSO). It is important not just to characterise these modes in present day climate, but also their potential future changes. Previous research suggests that these modes of variability are likely to undergo changes in their characteristics in response to increasing greenhouse gas concentrations and global warming (e.g. Branstator and Selten, 2009; Shepherd, 2014; Deser et al, 2018). Specifically, NAO variability is projected to strengthen under warming scenarios (Visbeck et al, 2001; Gillett et al, 2003; Deser et al, 2017; Huang et al, 2018; McKenna and Maycock, 2021). This strengthening is expected to increase the frequency of extreme positive NAO winters and their associated impacts in southern Europe (McKenna and Maycock, 2021). In contrast, future changes in ENSO variability remain somewhat uncertain, although an increase is suggested to be more likely than a decrease (Maher et al, 2018; Cai et al, 2021, 2022; Wengel et al, 2021; Planton et al, 2024). The spatial pattern of ENSO is also expected to change under warming, although there is considerable uncertainty regarding the nature of this change (e.g. Maher et al, 2018, 2023). Additionally, the Pacific North American (PNA) pattern is projected to amplify (Chen et al, 2018; O'Brien and Deser, 2023) and shift its center-of-action northeastward (Michel et al, 2020; O'Brien and Deser, 2023). The linkage between the PNA and NAO may also strengthen in the future by virtue of their mutual connection to ENSO (O'Brien and Deser, 2023; Beverley et al, 2024).

Teleconnections from modes of variability whereby a local perturbation results in a remote response (Wallace and Gutzler, 1981; Barnston and Livezey, 1987; Feldstein, 2000; Feldstein and Franzke, 2017), may also change in a warming climate. For example, atmospheric teleconnections driven by ENSO may be modified in response to changes in ENSO itself, and also to mean-state changes within the tropics and extratropics. For example, irrespective of changes in ENSO variance, precipitation variability associated with ENSO in the tropical Pacific is expected to increase (e.g. Power et al, 2013) and shift eastward as the mean state warms (e.g. Drouard and Cassou, 2019;

Zhou et al, 2014). In addition, mean-state changes in the position and strength of the midlatitude jet stream will alter ENSO-related teleconnections by modifying the sources and propagation characteristics of Rossby Waves. Indeed, ENSO teleconnections themselves are projected to change across approximately 50% of the globe, with most, but not all regions, experiencing an amplification of historical temperature and precipitation impacts (McGregor et al, 2022).

Understanding teleconnections and their projected changes, as well as what they mean for temperature and precipitation around the globe, is confounded by the lack of independence between different modes and their compounded impacts (e.g. O'Brien and Deser, 2023). For example, precipitation and temperature along the west coast of the United States are influenced by both the Pacific Decadal Oscillation (PDO) and ENSO (Maher et al, 2022), yet these modes are not independent of one another (Newman et al, 2016). Similarly, precipitation over Australia is affected by multiple modes of variability (Risbey et al, 2009), illustrating that understanding a single mode in isolation is not sufficient to fully explain local temperature and precipitation patterns. To further complicate matters, simply knowing the phase of each climate mode is often not enough to determine impacts. Indeed, modes of climate variability typically shift the likelihood of extreme events rather than serving as deterministic predictors (Maher et al, 2022). Despite these complexities, projecting changes in multiple modes of variability and their combined impacts remains essential for understanding the potential for extreme events and anticipating how local climate impacts are likely to evolve in the future.

To truly understand changes in variability and their time evolution in climate models, single model initial-condition large ensembles (SMILEs) are an invaluable tool (Deser et al, 2020; Kay et al, 2015; Maher et al, 2021a). These SMILEs are global coupled climate models, run with identical external forcing, identical model configuration, but different initial conditions for each ensemble member. The large number of ensemble members provides robust sampling of internal variability at any given time in each SMILE. As such these are ideal tools to investigate climate variability and it's response to external forcing.

A novel method to quantify evolving characteristics of modes of variability is the Snapshot Empirical Orthogonal Function Analysis (or ensemble EOF; Haszpra et al, 2020; Herein et al, 2016; Maher et al, 2018; O'Brien and Deser, 2023). This method permits the use of EOF's to quantify modes of variability at any given interval in time, using samples from all members of a given SMILE. This approach thus enables the identification of how the amplitude and spatial characteristics of a mode may change in time due to external forcing. This method was applied assess forced changes in the leading patterns of wintertime atmospheric circulation variability over the Northern Hemisphere (NH) in the 40-member Community Earth System Model version 1 (CESM1) SMILE (O'Brien and Deser, 2023). They found that internal modes of circulation variability in the North Pacific and Atlantic amplify, expand their spatial footprint and produce enhanced precipitation impacts as greenhouse gas forcing increases. Notably, the third North Pacific EOF (the "East Pacific Pattern") demonstrated the largest forced changes in CESM1, which has important implications for the climate along the United States (US) west coast, and in particular, California.

These changes were driven by teleconnections from amplified ENSO activity in the far eastern tropical Pacific and by intrinsic midlatitude atmospheric variability. Furthermore, the pattern of amplification of extratropical modes was found to resemble the pattern of changes in the mean-state, highlighting the link between mean-state shifts and variability.

One of the largest uncertainties in future projections of regional climate change comes from model-to-model differences (Maher et al, 2021b), particularly for variability (van der Wiel and Bintanja, 2021; Lee et al, 2021). In this study we extend the work of O'Brien and Deser (2023) to eight SMILEs from the new Multi-Model Large Ensemble Archive v2 (Maher et al, 2025) to investigate structural uncertainty in forced changes in leading modes of wintertime atmospheric circulation variability over the NH and their precipitation impacts.

2 Methods

While a traditional Empirical Orthogonal Function (EOF) analysis computes modes of variability across the time dimension of a single data set (observations or a single realisation of a climate model or SMILE), the Snapshot EOF (SEOF) methodology computes modes of variability across the ensemble dimension of a SMILE at each time step independently (Haszpra et al, 2020; Herein et al, 2016; Maher et al, 2018; O'Brien and Deser, 2023). Because each member of a given SMILE contains a unique sequence of internal variability (once memory of the initial conditions has been lost), the phases and amplitudes of a given mode are randomly distributed across the members, thereby providing the SEOF analysis a wide sampling at any given instant in time. For example, ENSO may be in a neutral, positive or negative phase, and may be strong or weak, in different members of a SMILE at a given time. To isolate internal variability in each member, the forced component is removed by subtracting the ensemble-mean at each timestep. To compute SEOFs at each timestep of a given SMILE we apply the following steps to the 500hPa geopotential height field in each member:

1. **Compute the December - Feburary (DJF) seasonal mean for each year of simulation**.
2. **Remove the ensemble mean** at each timestep to create anomalies (i.e. departures from the forced response) due to internal variability.
3. **Apply a cosine latitude weighting** to account for variations in grid cell area with latitude.
4. **Pool data from five consecutive DJF seasons** to increase sample size (assuming stationarity over the 5-year window).
5. **Compute SEOFs** of the pooled data using the anomalies from all ensemble members in a given SMILE.
6. **Assign the SEOF and its associated "Snapshot Principal Component" (SPC) result** to the central year of each pooled window.
7. **Ensure consistent sign** of each SEOF mode across time using a pattern correlation over the region of interest, correcting for potential ± 1 sign flips that can occur in EOF analysis.

8. **Create global regression maps** by linearly regressing anomalies (departures from the ensemble mean) of the relevant climate variable at each timestep on the standardised SPCs.

This methodology replicates O'Brien and Deser (2023), with further details available in the original study. We apply this method to the eight SMILEs listed in Table 1 to investigate the following modes of variability:

North Pacific (20°–90°N, 110°–260°E):

- **Mode 1:** Pacific–North American pattern (PNA; Barnston and Livezey, 1987)
- **Mode 2:** North Pacific Oscillation (NPO; Linkin and Nigam, 2008)
- **Mode 3:** East Pacific Pattern (EPP; Barnston and Livezey, 1987; Yuan et al, 2015)

North Atlantic (20°–90°N, 80°W–10°E):

- **Mode 1:** North Atlantic Oscillation (NAO; Hurrell et al, 2003). We note that Figures are shown opposite the traditional convention to match the visualisation in O'Brien and Deser (2023).

We also compute the two leading SEOFs of tropical Pacific sea surface temperatures (35°S–35°N, 140°–295°E):

- **Mode 1:** First component of the El Niño Southern Oscillation (ENSO) (Takahashi et al, 2011)
- **Mode 2:** Second component of ENSO (Takahashi et al, 2011)

Table 1 SMILEs used in this study. Note that qualitatively similar results are found for ACCESS-ESM1.5 and CanESM5 in SSP585 as compared to the SSP370 results presented in this study (not shown).

Model	CMIP	Future Scenario	Members	time period	Reference
MPI-GE	5	RCP8.5	100	1850-2099	(Maher et al, 2019)
MIROC6	6	SSP585	50	1850-2100	(Tatebe et al, 2019)
IPSL-CM6A	6	SSP370	10	1850-2100	(Boucher et al, 2020)
GFDL-SPEAR-MED	6	SSP585	30	1921-2100	(Delworth et al, 2020)
CanESM5	6	SSP370	25	1850-2100	(Swart et al, 2019)
ACCESS-ESM1.5	6	SSP370	40	1850-2100	(Ziehn et al, 2020)
CESM1	5	RCP8.5	40	1920-2100	(Kay et al, 2015)
CESM2	6	SSP370	100	1850-2100	(Rodgers et al, 2021)

3 Results

3.1 A multi-model perspective on projected forced changes in circulation and precipitation variability

Building on the results of O'Brien and Deser (2023), we take a multi-model approach to investigate projected changes in circulation variability and their consequent impacts

on precipitation. We first consider projected changes in circulation variability from the early 20th century to the late 21st century across all 8 SMILEs before decomposing the changes into distinct modes and assessing model performance relative to observations. Here, we define the early 20th century as the average of the SEOFs over the period 1924-1934, which will be used as the baseline period for all analysis. The late 21st century is defined as the average of the SEOFs over the period 2087-2097 (recall that the SEOFs are computed for each year separately using pooled anomalies over a centred 5-year window). In the early 20th century all models show hotspots of variability in the north Pacific and north Atlantic oceans that extend onto the nearby land surface (Figure 1; first column). All models except MIROC6 project a robust strengthening of the Aleutian low variability with most models also projecting a decrease in variability in the northern US and an increase in the south (Figure 1; third column). These consistent signals across models appear in the multi-ensemble mean (stippled regions in the bottom right panel of Figure 1). In contrast, models show a lack of consistency in the Atlantic basin and European sector. Projected precipitation variability is largely consistent across models in both the Pacific and Atlantic basins and over the entire North American Continent (Figure 2; agreement shown in stippling) with an increase on both eastern and western US coastlines, the North Pacific and mid latitude Atlantic, and generally all NH land masses. Conversely precipitation variance decreases in all models in both the subtropical Atlantic and east Pacific. Changes in precipitation variability are due to the combination of the changes in circulation variability and the mean effects of warming on the hydrological cycle (e.g. enhanced water vapor content in regions of strengthened ascent in the extratropics and deep tropics following the Clausius-Clapeyron relationship, and reduced moisture in the subtropics due to enhanced subsidence). The stippling in Figure 2, which represents model agreement (7 out 8 models agree on the sign of the change) is much more widespread and consistent compared to Figure 1. This suggests that precipitation variability change is less model dependent than the circulation variability change, leading us to the conclusion that the thermodynamic effects of warming on precipitation variability dominate circulation-induced changes in precipitation variability. We do additionally note the high model-agreement in Figure 1 in the Northern Pacific, which likely also contributes to the precipitation variability agreement and change.

3.2 Modes of Circulation Variability: Model evaluation

Before examining future changes, we compare the simulated modes of Z500 variability with observations to assess their realism. For this comparison we use a traditional EOF approach (i.e. EOFs in time averaged across ensemble members) based on the period 1950-2015 so as to treat the SMILEs and observations in the same manner. However, we note that the traditional and SEOF approaches yield very similar results for the SMILEs (see Figure S2). All modes of variability are presented following the phase conventions in O'Brien and Deser (2023). The spatial pattern of the leading EOF in the North Pacific (PNA) and North Atlantic (NAO), obtained by regressing DJF Z500 anomalies onto the correponsing standardised PC timeseries, compares well with observations in all eight SMILEs (Figure 3). The high pattern correlations (ranging from 0.79-0.92 for the PNA and 0.85-0.94 for the NAO) between observations and each

SMILE attests to the realism of the simulated PNA and NAO structures. The second mode in the North Pacific (NPO) is also well represented at the large scale, although some discrepancies appear along the western US coastline. The pattern correlations for the NPO are somewhat lower than those for the PNA and NAO (ranging from 0.7 to 0.84 across the SMILEs). Of the eight models, only MIROC6 captures both the observed pattern and magnitude of the NPO, while ACCESS-ESM1.5 and CESM1 & 2 reproduce the correct pattern, but underestimate the magnitude. The third EOF in the North Pacific (EPP) is again captured at the large scale, but model results differ from each other and from observations, with models generally displaying a westward shift in the pattern relative to the observed one (pattern correlations range from 0.02-0.71).

While the large-scale patterns are generally well captured for all North Pacific and North Atlantic modes considered, it is important to recognise that observations represent just one realisation of the climate system (Maher et al, 2025). Therefore, to make a fair comparison with the SMILEs, we must assess whether any individual ensemble member resembles observations rather than considering just the mean across members. This comparison is shown in the Taylor diagrams in Figure 4. For the PNA, NPO and NAO, all models have ensemble members that match observations well across all metrics (correlation coefficient, standard deviation, and RMSD) highlighting that all models well-represent these modes of variability. Specifically, for both the PNA and NPO, CESM2, MPI-GE, ACCESS-ESM1.5, CESM1, and GFDL-SPEAR have members close to the observations (correlation coefficients greater than 0.9, similar standard deviaiations to observations and RMSD below 5). For the NAO, all models have ensemble members that are close to observations, except for CanESM5 in which all members have RMSD larger than 7.5, too high standard deviations, and correlations lower than 0.95, while all other models have members higher than 0.95. For the EPP, there is a wide range of correlation values across the members of each SMILE (ranging from negative to positive), suggesting that this mode is less well-constrained (i.e. we may need a longer record to sufficiently capture this mode in observations). Even so, all models have members relatively close to observations (similar standard deviations, correlation coefficients around 0.9, and RMSD less than 5) except CESM1 and ACCESS-ESM1.5. We note that observations are just one realisation and as such if some members have low correlations with observations it does not mean they do not well represent observations. However, for a model to be potentially considered as having a realistic representation of the mode in question, it must have at least some ensemble members that show high correlations with observations. Based on this point, if some members of a SMILE show high correlations, then this model can be considered to have a realistic representation of the mode in question, subject to uncertainties due to limited sampling.

Overall for all models considered, while biases exist, nearly all models have ensemble members that compare well with observations, and no single model clearly outperforms or underperforms compared to the others. Therefore, we include all eight SMILEs in our subsequent analysis to capture a robust range of future projections and identify areas of model agreement.

3.3 Modes of Circulation Variability: Projected changes

To understand what drives the projected changes in circulation and precipitation variability shown in Figures 1 and 2, we apply the SEOF method to identify dominant modes of NH Z500 variability and investigate their projected changes (Figure 5). For each mode, the positive phase in the early period (1924-1934) is shown as contours, and the difference between the positive phase in the late period (2087-2097) and positive phase in the early period is shown as color shading. For example, for SEOF1, dashed contours and blue shading over the North Pacific region indicate that the positive phase of the PNA during the early period (characterised by a deeper-than-normal Aleutian Low; denoted by the strong negative blue coloured anomalies) is projected to intensify (become even deeper; a darker blue colour in the Figure), and vice versa for the negative phase. The main center of action of the PNA is projected to intensify in all models except CESM2 and MIROC6, although the amplitude of the projected amplification varies considerably across models (smallest for ACCESS and largest for IPSL-CM6A). Remote linkages over the North Atlantic and European sector are highly model dependent. To summarize the robustness of the projected changes across the 8 SMILEs, we compute a signal-to-noise ratio (S/N) defined as the multi-model mean change divided by the standard deviation across models. A S/N value exceeding 1 highlights regions where there is high inter-model agreement on the projected change relative to the spread across models. For the PNA the S/N exceeds 1 over the northern portion of the North Pacific and exceeds 2 over the Gulf of Mexico and Florida. We note that the MEM and S/N are qualitatively similar when MIROC6 and CESM2 are removed (not shown), highlighting that it is not just these outliers that drive the model differences. Large inter-model differences are found in the Atlantic, where the projected influence of the PNA is inconsistent.

The NPO, shows substantial model disagreement in its projected circulation impacts over the Pacific and the continental US. For example there is a strong intensification of it's influence over Alaska in CanESM5 and MPI-GE, but a small weakening in MIROC6 and CESM1. Some models (e.g. CESM2, CESM1, GFDL-SPEAR and MIROC6) show an intensification of the circulation over the south-eastern US related to the NPO while the other models show a weakening (e.g. MPI-GE and CanESM5). The influence of the NPO on the Atlantic, however, appears relatively consistent with a strengthening influence in the mid-latitudes and a weakening in both the tropics and high-latitudes further demonstrated by the S/N exceeding 1 in this region. This mode also has increasing links to the tropics again demonstrated by the S/N larger than 1.

For the EPP there is some agreement among models, particularly over the west coast of the US associated with a projected eastward shift of the pattern, highlighted by the zonal dipole of high S/N between the Pacific and western US. Finally, the NAO exhibits high inter-model variability in its projected changes, especially over the Atlantic, as indicated by a low S/N in this region. Specifically, CanESM5 and IPSL-CM6A show similarities in the change with a strong weakening of the NAO circulation (red region highlighting a decrease due to the sign of the historical circulation), however the other models show weaker and inconsistent changes in sign across the region. This is likely the cause of the model differences found in Figure 1 in the Atlantic.

Interestingly, projected changes in NAO variability are consistently linked to a projected intensification of Aleutian Low variability associated with the PNA and to the enhanced variability in the tropics, with S/N values exceeding one in these areas. This highlights the bi-directional link between the Atlantic and Pacific as shown by the influence of the changes in the North Pacific EOFs on the Atlantic and visa versa, which are different in strength in each model.

Changes in atmospheric circulation variability lead to corresponding shifts in local precipitation variability. To explore these impacts, we regress precipitation onto the Z500 SPCs and plot the change in the regressed precipitation field in the late compared to early period (Figure 6). The projected intensification and eastward-shift of the Aleutian Low center-of-action of the PNA pattern leads to enhanced precipitation variability over the eastern North Pacific and along the west coast of the US and diminished precipitation variability over the central North Pacific in most models. This signal is notably absent in MIROC6, where the Aleutian Low variability does not increase. The magnitude of the projected precipitation variability increase has high S/N showing the MEM change is larger than the model differences. The Pacific sector of the Arctic is another region of high S/N (values greater than 2), indicative of a robust reduction in precipitation variability associated with the PNA in the future, in line with the agreement in the changes in the PNA itself (Figure 5; bottom left). In line with the lack of model agreement in the projected behaviour of the NPO over the eastern North Pacific and North America, NPO-related precipitation changes in these regions also vary substantially between models, reflected in low S/N. However, the consistent NPO projections over the far western Pacific centered near Japan and over the North Atlantic produce robust (S/N greater than 1) signals in precipitation variability along the Kuroshio Extension and in a meridional dipole pattern over the North Atlantic. The high degree of model consistency in projected EPP variability is evident in the associated precipitation impacts, with most models projecting a banded structure of increased precipitation variability along the US West Coast, extending southwestward to Hawaii, decreased precipitation variability from British Columbia to the central north Pacific, and enhanced variability in the far northwestern Pacific. These changes likely stem from shifts in the jet stream position, supported by the shift in precipitation across the Pacific seen in both individual models and the MEM. We note that the details of the location of this change are shifted somewhat in each model, resulting in the S/N being lower than expected in this region. While there is a lack of model consensus on the projected changes in NAO-related precipitation variability over the central and northern North Atlantic, consistent with the Z500 field itself, the southwestern North Atlantic and the Pacific near Hawaii are regions of strongly robust (S/N greater than 2) changes.

One of the advantages of the SEOF method is that projected changes in the characteristics of internal variability can be evaluated continuously through time. In Figure 7 (left and right columns), we present the total and explained variance of each Z500 mode as a function of time from the beginning of each simulation until the end of the century. In the North Pacific, total Z500 variance increases continuously in all models except ACCESS-ESM1-5 and MIROC6, where it initially increases but subsequently declines (red curves Figure 7, left column). The proportion of variance

explained by each of the three North Pacific Z500 modes remains relatively stable over time, although the PNA shows an increase in most models (excluding ACCESS, IPSL-CM6A and MIROC6 where it stays relatively stable). In contrast, the NAO exhibits less agreement across models, with some showing increasing total variance (CESM1 with a 15% increase, MIROC6 with 10%), others a decreasing (CESM2 with a 10% decrease, ACCESS with 15%, CanESM5 with 20%), and some showing little change (GFDL-SPEAR, IPSL-CM6A and MPI-GE). Despite these differences, the percentage of the variance explained by the NAO remains fairly stable across all models over time.

3.4 Role of the Tropical Pacific

Models show substantial differences in their projections of ENSO (Maher et al, 2023), which could contribute to the differences in their future circulation changes, as ENSO teleconnections can project onto the NH modes of variability (O'Brien and Deser, 2023). These model differences in ENSO projections are highlighted in Supplementary Figure S9 (left hand side). In particular, the different models show contrasts in sign in their projected surface temperature changes in the tropical Pacific as well as low signal to noise in the region. We note that the precipitation related changes to these modes in the tropical Pacific are much more consistent (Supplementary Figure S9; right hand side), as noted in previous work (Power et al, 2013). The total variance (Figure 7) of tropical Pacific SST EOFs broadly agrees with (Maher et al, 2023) who found that most models exhibit a time-dependent increase in tropical Pacific SST variability. While most models show a projected increase in tropical Pacific SST variability, notable exceptions include MPI-GE, which shows no change, and CESM2 and GFDL-SPEAR, which increase and then decrease, with CESM2 returning to it's 1850 amplitude by the end of the century from a high in the 2020s. Interestingly, several models show a plateau in variance at the end of the record, suggesting a possible future decline if simulations were extended. The variance explained by each EOF tends to follow the trajectory of total variance.

To investigate how changes in the tropical Pacific modes impact the extratropical Z500 modes, we linearly regress the Z500 anomalies over the NH onto the two leading standardised SPCs of tropical Pacific SSTs at each timestep and then remove this contribution from the Z500 field following O'Brien and Deser (2023). We then recompute the Z500 SEOFs using this residual field from which the tropical Pacific influence has been removed. We find that for all models, the total variance of the "tropical Pacific removed" Z500 anomalies over the North Pacific is substantially reduced compared to the full Z500 anomalies, while the percent variance explained by each SEOF mode remains similar (Figure 7, dashed curves in the left column). In the Atlantic, the total variance during the historical portion of the simulations decreases only slightly without the influence of the tropical Pacific, while the future variance is significantly reduced (in all models except IPSL-CM6A and MIROC6), suggesting that the tropical Pacific's influence on the Atlantic intensifies in future projections across all models. Similar to the Pacific modes, the percent variance explained by the NAO is relatively insensitive to the removal of tropical Pacific influence in all models (Figure 7, right column).

Figure 8 shows the spatial patterns of Z500 and precipitation regressed onto the two leading standardized SPCs of tropical Pacific SSTs (TPac) in the early period (contours) and their future change (late minus early periods; shading) in each SMILE and the MEM. While the early period Z500 teleconnection associated with TPac SEOF1 is robust across models and resembles the PNA pattern, the projected change in the teleconnection shows substantial model disagreement in both pattern and sign (Figure 8, left column). Notably, CESM2, GFDL-SPEAR and MIROC6 show a future weakening of the teleconnection variability (denoted by positive Z500 variability values; red shading) over the central North Pacific while CanESM5, IPSL-CM6A and MPI-GE show the opposite behaviour. This does not appear to be linked to the change in variance in the TPac (Figure 7). Model differences in the sign of the future changes in Z500 variability are also found over the North Atlantic. As highlighted in the S/N maps, model differences in future Z500 variability changes associated with TPac SEOF1 are largest over the western and central North Pacific (low S/N) and smallest in the eastern North Pacific, southeastern US and across the Atlantic along around 30N and approximately 60N (high S/N). Corresponding differences are found in the precipitation responses (Figure 8; third column), which show large model differences in the same regions as the model differences in circulation. In contrast, TPac SST SEOF2 shows more consistent behaviour in projected changes in its Z500 teleconnections across models with enhanced Z500 variability in the Aleutian Low region (Figure 8; second column) with high S/N. This in turn corresponds to increased precipitation variability along the southwestern US coast (Figure 8; far right column), which also has a high S/N ratio.

Given the lack of independence between tropical Pacific SST SEOFs and NH Z500 SEOFs, and the large model differences in tropical Pacific projections outlined above, we test whether these tropical differences drive the spread in projections of leading modes of Z500 variability over the NH. To do so, we compare the projected changes in the SEOFs based on the full Z500 field with those obtained from the residual Z500 field after removing the influence of the tropical Pacific SST SEOFs via linear regression. Results from the individual SMILEs are shown in Figures S10 & S11. Here we focus on the MEM results (Figure 9). The projected amplification of the MEM PNA is considerably reduced when the influence of the tropical Pacific is removed (Figure 9, upper two panels in the left column). The multi-ensemble standard deviation (ME-STD), which reveals where models differ most in their projections also decreases when the tropical Pacific is removed, not only over the North Pacific and North America, but also over the North Atlantic (Figure 9, middle two panels in left column). Given that both the signal and noise reduce for the PNA, the S/N over the North Pacific is largely unchanged; however, the S/N increases across the eastern US, tropical North Atlantic and northern Europe due mainly to a reduction in the noise rather than an augmentation of the signal (Figure 9, lower two panels in the left column). We find a similar story for the PNA driven precipitation (Figure 10), although in this case the S/N increases over the North Pacific and western Arctic and decreases over the western US when the tropical Pacific influence is removed.

For the NPO, removing the influence of the tropical Pacific decreases the S/N in the Atlantic region and throughout the tropical belt due to a stronger reduction in the MEM signal compared to the ME-STD noise (Figure 9, second column). While the

NPO driven precipitation also shows a decrease in the S/N over the Atlantic sector when the tropical Pacific influence is removed, due to a larger decrease in the signal than the noise, there are also slight increases in S/N over the Gulf of Alaska and the eastern US seaboard (Figure 10, second column).

For the EPP, removing the tropical Pacific influence reduces the S/N over western North America as a result of the larger increase in noise than signal, while it increases the S/N over the eastern US and tropical North Atlantic as a result of reduced noise and larger signal, for both circulation and precipitation (Figure 9 & 10, third column).

For the NAO, removing the tropical Pacific influence slightly augments the S/N in the circulation centres-of-action over the western North Atlantic and European continent due mainly to the enhanced signal, while it greatly reduces the S/N over the North Pacific and the tropical belt due to the decreased signal (Figure 9, far right column). Analogous results are found for NAO-related precipitation, although the increase in S/N over the Atlantic/European sector is not as apparent (Figure 10, far right column).

We summarize the magnitude of the future change in each Z500 SEOF mode, with and without the influence of the Tropical Pacific, based on the MEM (Figure 11). The magnitude of future change is quantified by computing the spatial root mean square (RMS) of the future change in Z500 regressions (shaded fields in the upper two rows of Figure 9 for the MEM) over the domain used to define the SEOF (North Pacific or North Atlantic). For the MEM PNA the magnitude of the circulation variability is projected to increase, with approximately half of the increase due to the influence of the tropical Pacific.

In contrast, the MEM NAO variability is projected to weaken, and removing the tropical Pacific influence approximately doubles the amplitude of the weakening. This is consistent with the opposite sign of NAO variability in the early 20th century compared to its future change (compare contours and shading in Figure 9, last column, top 2 rows) and borne out by the enhanced signal-to-noise when the tropical Pacific influence is removed (Figure 9, last column, bottom 2 rows). Also of note is the stronger co-location of the NAO variability centers-of-action in the early 20th century (contours) and their future changes (shading) after removing the tropical Pacific influence (compare top 2 rows in the last column of Figure 9). The projected increase in the magnitude of the MEM NPO, although smaller than that of the PNA, is more than doubled when the influence of the tropical Pacific is removed. Finally, while the EPP RMS is projected to decrease, this is found to be entirely due to the tropical Pacific with no changes remaining after it's removal. Thus, future changes in tropical Pacific SST variability exert a large influence on future changes in the amplitude of the MEM Z500 SEOF modes, augmenting the PNA, offsetting the NPO and NAO, and dominating the EPP.

3.5 Impacts on Californian and South-Eastern US precipitation variability

We additionally consider the impacts of each Z500 mode of variability on Californian precipitation variability to assess whether the projected changes in precipitation variability are consistent across models. We find a projected increase in Californian

precipitation variability associated with the PNA and NAO (Figure 12; left), about two-thirds which is directly attributable to changes in tropical Pacific SST variability for both modes. In contrast, projected changes in the NPO exert only a minor influence on Californian precipitation variability, regardless of whether the tropical Pacific influence is removed or not. Projections of precipitation variability driven by the EPP are as large as those due to the PNA when the influence of the tropical Pacific is included. When the confounding influence of this region is removed, an even larger increase in Californian precipitation variability emerges due to the EPP alone. This suggests that the projected increases in Californian precipitation variability attributed to the PNA and NAO are in fact driven in large part by non-independent changes in tropical Pacific SST variability whose associated Z500 teleconnections project onto these modes. Conversely, the tropical Pacific masks approximately one-third of the signal from the EPP, highlighting that the EPP itself is projected to drive increased volatility of Californian precipitation variability in the future. We also consider the south-east US (Figure 12; right) which shows contrasting results to Californian precipitation variability. An increase in precipitation variability in this region due to the PNA, EPP and NAO and a decrease due to the NPO are all found to be related to tropical Pacific changes. When the tropical Pacific is removed, the PNA and NAO changes switch to a decrease of the same magnitude, the NPO change results in an increase of two-thirds the magnitude of it's original decrease, and the EPP influence is reduced to one-third of it's original magnitude. These results highlight the key role of the tropical Pacific in masking the influence of the other modes in this region.

4 Discussion

While our results show that the SMILEs considered in this study generally perform well in simulating the leading modes of wintertime circulation variability in the NH during the period 1950-2015, we find that this alone is not sufficient to ensure consistent projections of these modes and their associated impacts over the 21st Century. Where model disagreement is evident (in particular in the NPO and NAO), it reflects our ongoing inability to fully understand and simulate the processes that will change under warming. This highlights the continued need for a diversity of climate models to adequately capture the range of possible futures, especially in areas where our understanding is currently limited. Longer observational records will help improve model evaluation and allow for better quantification of internal variability and updated evaluation methods (Suarez-Gutierrez et al, 2021; Simpson et al, 2025), while higher-resolution simulations may better capture key processes (Wengel et al, 2021; Chang et al, 2026). However, our understanding remains incomplete regarding the precise sources of model differences. In this paper, we identify the large differences in the projected changes in SST variability in the tropical Pacific (e.g. ENSO) as a key driver of model differences in projected changes in Z500 variability over the NH, but also show that they are not the only source of discrepancy.

The SEOF approach applied to SMILEs provides a direct and concise way to assess forced changes in modes of circulation variability as highlighted by O'Brien and

Deser (2023). While informative O'Brien and Deser (2023) was limited to one particular SMILE (CESM1), leaving open the possibility that different SMILEs might behave differently. We address this gap in our study and and also evaluate model realism in simulating modes of variability over the historical record using the traditional time-EOF approach. Similar to previous studies (Michel et al, 2020; Chen et al, 2018; O'Brien and Deser, 2023), we find a projected future strengthening and north-easterly shift of the variability of the Aleutian low associated with the PNA pattern in all models except MIROC6 (see Figure 5), highlighting a broad consistency across models. When the influence of the tropical Pacific is removed, the spread in projections decreases, indicating that some of the inter-model differences, particularly in the Aleutian low region, are driven by inconsistencies in how the tropical Pacific is changing. Notably, the increasing influence of the PNA on Californian precipitation variability is found to be driven in large part by the tropical Pacific in the MEM (Figure 12). When isolated, the intrinsic atmospheric PNA changes themselves have limited impact on Californian precipitation, reinforcing the importance of accounting for interactions between modes of variability in future projections to truly understand what drives what.

Our results showing model disagreement in the projections of the NPO are consistent with previous work using CMIP5 models, further highlighting persistent uncertainty in this mode (e.g. Chen et al, 2018, 2021). Removing the influence of the tropical Pacific leads to greater consistency in both circulation and precipitation projections across models, particularly over the western US coastline, Alaska, and the continental US. However, even with the tropical Pacific influence removed, notable model differences remain. This suggests that uncertainties in the NPO's future behaviour stem from factors beyond tropical Pacific variability and that further work is needed to better understand the processes driving the NPO and how they may change under warming.

Similar to the findings of O'Brien and Deser (2023), we diagnose an important role for the EPP in influencing precipitation along the western US coastline. Markedly, this mode drives precipitation variability changes that are not solely driven by the tropical Pacific. In particular, for the EPP, we find a consistent increase in its influence on Californian precipitation in the future across all models, a response that is clouded by the tropical Pacific influence. This result, again in line with O'Brien and Deser (2023), points to a growing importance of the EPP for US regional hydroclimate under future climate change.

The NAO also exhibits substantial discrepancies in future projections across models, consistent with previous work (e.g. Smith et al, 2025). These discrepancies cannot be attributed to tropical Pacific influences, indicating that the differences arise from the NAO projections themselves. All models suggest that the tropical Pacific will exert a stronger influence on the Atlantic variability in the future (i.e. a larger reduction in total variance in the NAO region when the tropical Pacific is removed), with three potential mechanisms for this change are presented in Drouard and Cassou (2019). Furthermore, models do not agree on future changes in variance for the NAO, reinforcing the idea that this mode remains a key source of uncertainty.

Finally, our projections for the tropical Pacific are in agreement with earlier findings (Maher et al, 2023), showing model-dependent changes over time. These include known biases in tropical Pacific variability, consistent with those identified by Planton et al (2021) and Bellenger et al (2014), and contribute to the broader uncertainty in teleconnection patterns under climate change.

5 Conclusions

In summary, we find the following:

1. Climate models generally capture the key modes of atmospheric circulation variability in the North Pacific and North Atlantic, with well-known biases remaining in the modes of tropical Pacific SST variability (Figures 3, 4 & S1).
2. There is limited model agreement on projections of the NPO and NAO. While some of the model disagreement in the NPO can be attributed to differences in tropical Pacific variability, this does not fully account for the spread (Figures 5, 9 & 11).
3. Most models agree on projected changes in the PNA, which are largely associated with an intensification of the Aleutian low variability. Where this intensification does not occur (e.g. in MIROC6), it can be linked to different behaviour in tropical Pacific variability (Figures 5, 9, 11 & S10).
4. The EPP is found to contribute to a consistent increase in precipitation variability over California in future projections, suggesting that its influence on this region will strengthen in a warming climate (Figure 12).
5. The effect of all four circulation modes of variability on the south-east US precipitation is masked by the tropical Pacific (Figure 12).
6. Strong links between modes and across basins underscore the difficulty of isolating the effects of individual modes. This highlights the interconnected nature of the climate system (Figures 5, 6, 9, 10).
7. The percentage of variance explained by each mode remains relatively stable in the future, although the total variance may increase or decrease depending on the region and model (Figure 7).
8. Projected precipitation changes are strongly linked to changes in the behaviour and influence of circulation modes, reflecting both direct thermodynamic responses to warming and dynamically mediated impacts (Figures 1, 2).

Acknowledgements. NM was supported by the Australian Research Council Discovery Early Career Researcher Award DE230100315. We would like to acknowledge computing support from the Casper system (https://ncar.pub/casper) provided by the National Science Foundation (NSF) National Center for Atmospheric Research (NCAR), sponsored by NSF. We additionally thank Adam Phillips (NSF-NCAR) for providing observational data and guidance. CD is supported by NSF-NCAR. Support for the Twentieth Century Reanalysis Project version 3 dataset is provided by the U.S. Department of Energy, Office of Science Biological and Environmental Research (BER), by the National Oceanic and Atmospheric Administration Climate Program Office, and by the NOAA Earth System Research Laboratory Physical Sciences Laboratory.

Competing Interests. The authors declare no competing interests.

Data availability. SMILE data used in this study is publicly available via the Multi-model large ensemble archive version 2 (MMLEAv2) at https://www.cesm.ucar.edu/community-projects/mmlea/v2.

Code availability. All final code can be found at: https://github.com/nicolamaher/SEOF.

Funding. This word was funded by the Australian Research Council Discovery Early Career Researcher Award DE230100315.

Author contribution. This project was co-designed by NM, CD and JPO as a follow up to a previous study by JPO and CD. NM led the project, created the figures and wrote the manuscript. CD and JPO provided input and ideas for the Figures, methods, and helped to synthesise the results. The SEOF code used in the paper was originally written by JPO and modified for use with multiple SMILEs by NM. All authors contributed to the final manuscript.

References

Barnston AG, Livezey RE (1987) Classification, seasonality and persistence of low-frequency atmospheric circulation patterns. Monthly Weather Review 115(6):1083 – 1126. https://doi.org/10.1175/1520-0493(1987)115⟨1083:CSAPOL⟩2.0.CO;2, URL https://journals.ametsoc.org/view/journals/mwre/115/6/1520-0493_1987_115_1083_csapol_2_0_co_2.xml

Bellenger H, Guilyardi E, Leloup J, et al (2014) Enso representation in climate models: from cmip3 to cmip5. Climate Dynamics 42(7):1999–2018. https://doi.org/10.1007/s00382-013-1783-z, URL https://doi.org/10.1007/s00382-013-1783-z

Beverley JD, Collins M, Lambert FH, et al (2024) Drivers of changes to the enso–europe teleconnection under future warming. Geophysical Research Letters 51(10):e2023GL107957. https://doi.org/https://doi.org/10.1029/2023GL107957, URL https://agupubs.onlinelibrary.wiley.com/doi/abs/10.1029/2023GL107957, e2023GL107957 2023GL107957, https://agupubs.onlinelibrary.wiley.com/doi/pdf/10.1029/2023GL107957

Boucher O, Servonnat J, Albright AL, et al (2020) Presentation and Evaluation of the IPSL-CM6A-LR Climate Model. Journal of Advances in Modeling Earth Systems 12(7):e2019MS002010. https://doi.org/https://doi.org/10.1029/2019MS002010, URL https://agupubs.onlinelibrary.wiley.com/doi/abs/10.1029/2019MS002010, e2019MS002010 10.1029/2019MS002010, https://agupubs.onlinelibrary.wiley.com/doi/pdf/10.1029/2019MS002010

Branstator G, Selten F (2009) "modes of variability" and climate change. Journal of Climate 22(10):2639 – 2658. https://doi.org/10.1175/2008JCLI2517.1, URL https://journals.ametsoc.org/view/journals/clim/22/10/2008jcli2517.1.xml

Cai W, Santoso A, Collins M, et al (2021) Changing el niño-southern oscillation in a warming climate. Nature Reviews Earth Environment 2(9):628–644. https://doi.org/10.1038/s43017-021-00199-z, URL https://doi.org/10.1038/s43017-021-00199-z

Cai W, Ng B, Wang G, et al (2022) Increased enso sea surface temperature variability under four ipcc emission scenarios. Nature Climate Change 12(3):228–231. https://doi.org/10.1038/s41558-022-01282-z, URL https://doi.org/10.1038/s41558-022-01282-z

Chang P, Fu D, Liu X, et al (2026) Future extreme precipitation amplified by intensified mesoscale moisture convergence. Nature Geoscience 19(1):33–41. URL https://doi.org/10.1038/s41561-025-01859-1

Chen S, Yu B, Wu R, et al (2021) The dominant north pacific atmospheric circulation patterns and their relations to pacific ssts: historical simulations and future projections in the ipcc ar6 models. Climate Dynamics 56(3):701–725. URL https://doi.org/10.1007/s00382-020-05501-1

Chen Z, Gan B, Wu L, et al (2018) Pacific-north american teleconnection and north pacific oscillation: historical simulation and future projection in cmip5 models. Climate Dynamics 50(11):4379–4403. URL https://doi.org/10.1007/s00382-017-3881-9

Delworth TL, Cooke WF, Adcroft A, et al (2020) SPEAR: The Next Generation GFDL Modeling System for Seasonal to Multidecadal Prediction and Projection. Journal of Advances in Modeling Earth Systems 12(3):e2019MS001895. https://doi.org/https://doi.org/10.1029/2019MS001895

Deser C, Hurrell JW, Phillips AS (2017) The role of the north atlantic oscillation in european climate projections. Climate Dynamics 49(9):3141–3157. URL https://doi.org/10.1007/s00382-016-3502-z

Deser C, Simpson IR, Phillips AS, et al (2018) How well do we know enso's climate impacts over north america, and how do we evaluate models accordingly? Journal of Climate 31(13):4991 – 5014. https://doi.org/10.1175/JCLI-D-17-0783.1, URL https://journals.ametsoc.org/view/journals/clim/31/13/jcli-d-17-0783.1.xml

Deser C, Lehner F, Rodgers KB, et al (2020) Insights from earth system model initial-condition large ensembles and future prospects. Nature Climate Change 10(4):277–286. https://doi.org/10.1038/s41558-020-0731-2

Drouard M, Cassou C (2019) A modeling- and process-oriented study to investigate the projected change of enso-forced wintertime teleconnectivity in a warmer world. Journal of Climate 32(23):8047 – 8068. https://doi.org/10.1175/JCLI-D-18-0803.1, URL https://journals.ametsoc.org/view/journals/clim/32/23/jcli-d-18-0803.1.xml

Feldstein SB (2000) The timescale, power spectra, and climate noise properties of teleconnection patterns. Journal of Climate 13(24):4430 – 4440. https://doi.org/10.1175/1520-0442(2000)013⟨4430:TTPSAC⟩2.0.CO;2, URL https://journals.ametsoc.org/view/journals/clim/13/24/1520-0442_2000_013_4430_ttpsac_2.0.co_2.xml

Feldstein SB, Franzke CLE (2017) Atmospheric Teleconnection Patterns, Cambridge University Press, p 54–104

Gillett NP, Graf HF, Osborn TJ (2003) Climate Change and the North Atlantic Oscillation, American Geophysical Union (AGU), pp 193–209. https://doi.org/https://doi.org/10.1029/134GM09, URL https://agupubs.onlinelibrary.wiley.com/doi/abs/10.1029/134GM09, https://agupubs.onlinelibrary.wiley.com/doi/pdf/10.1029/134GM09

Haszpra T, Herein M, Bódai T (2020) Investigating enso and its teleconnections under climate change in an ensemble view – a new perspective. Earth System Dynamics 11(1):267–280. https://doi.org/10.5194/esd-11-267-2020, URL https://esd.copernicus.org/articles/11/267/2020/

Herein M, Márfy J, Drótos G, et al (2016) Probabilistic concepts in intermediate-complexity climate models: A snapshot attractor picture. Journal of Climate 29(1):259 – 272. https://doi.org/10.1175/JCLI-D-15-0353.1, URL https://journals.ametsoc.org/view/journals/clim/29/1/jcli-d-15-0353.1.xml

Huang B, Thorne PW, Banzon VF, et al (2017) Extended reconstructed sea surface temperature, version 5 (ersstv5): Upgrades, validations, and intercomparisons. Journal of Climate 30(20):8179 – 8205. https://doi.org/10.1175/JCLI-D-16-0836.1, URL https://journals.ametsoc.org/view/journals/clim/30/20/jcli-d-16-0836.1.xml

Huang Y, Ren HL, Chadwick R, et al (2018) Diagnosing changes of winter nao in response to different climate forcings in a set of atmosphere-only timeslice experiments. Atmosphere 9(1). https://doi.org/10.3390/atmos9010010, URL https://www.mdpi.com/2073-4433/9/1/10

Hurrell JW, Kushnir Y, Ottersen G, et al (2003) An Overview of the North Atlantic Oscillation, American Geophysical Union (AGU), pp 1–35. https://doi.org/https://doi.org/10.1029/134GM01, URL https://agupubs.onlinelibrary.wiley.com/doi/abs/10.1029/134GM01, https://agupubs.onlinelibrary.wiley.com/doi/pdf/10.1029/134GM01

Kay JE, Deser C, Phillips A, et al (2015) The Community Earth System Model (CESM) Large Ensemble Project: A Community Resource for Studying Climate Change in the Presence of Internal Climate Variability. Bulletin of American Meteorological Society 96(8):1333–1349. https://doi.org/10.1175/BAMS-D-13-00255.1

Lee JJ.-Y., Marotzke, Bala G, et al (2021) Climate Change 2021: The Physical Science Basis. Contribution of Working Group I to the Sixth Assessment Report of the

Intergovernmental Panel on Climate Change, Cambridge University Press, chap Future Global Climate: Scenario-Based Projections and NearTerm Information, pp 553–672. https://doi.org/10.1017/9781009157896.006

Linkin ME, Nigam S (2008) The north pacific oscillation–west pacific teleconnection pattern: Mature-phase structure and winter impacts. Journal of Climate 21(9):1979 – 1997. https://doi.org/10.1175/2007JCLI2048.1, URL https://journals.ametsoc.org/view/journals/clim/21/9/2007jcli2048.1.xml

Maher N, Matei D, Milinski S, et al (2018) ENSO Change in Climate Projections: Forced Response or Internal Variability? Geophysical Research Letters 45:11,390–11,398. https://doi.org/10.1029/2018GL079764

Maher N, Milinski S, Suarez-Gutierrez L, et al (2019) The Max Planck Institute Grand Ensemble: Enabling the Exploration of Climate System Variability. Journal of Advances in Modeling Earth Systems 11(7):2050–2069. https://doi.org/10.1029/2019MS001639

Maher N, Milinski S, Ludwig R (2021a) Large ensemble climate model simulations: introduction, overview, and future prospects for utilising multiple types of large ensemble. Earth System Dynamics 12(2):401–418. https://doi.org/10.5194/esd-12-401-2021, URL https://esd.copernicus.org/articles/12/401/2021/

Maher N, Power SB, Marotzke J (2021b) More accurate quantification of model-to-model agreement in externally forced climatic responses over the coming century. Nature Communications 12(1):788. URL https://doi.org/10.1038/s41467-020-20635-w

Maher N, Kay JE, Capotondi A (2022) Modulation of enso teleconnections over north america by the pacific decadal oscillation. Environmental Research Letters 17(11):114005. https://doi.org/10.1088/1748-9326/ac9327, URL https://dx.doi.org/10.1088/1748-9326/ac9327

Maher N, Wills RCJ, DiNezio P, et al (2023) The future of the el niño–southern oscillation: using large ensembles to illuminate time-varying responses and inter-model differences. Earth System Dynamics 14(2):413–431. https://doi.org/10.5194/esd-14-413-2023, URL https://esd.copernicus.org/articles/14/413/2023/

Maher N, Phillips AS, Deser C, et al (2025) The updated multi-model large ensemble archive and the climate variability diagnostics package: New tools for the study of climate variability and change. Geoscientific Model Decelopment 18:6341–6365. https://doi.org/https://doi.org/10.5194/gmd-18-6341-2025

McGregor S, Cassou C, Kosaka Y, et al (2022) Projected enso teleconnection changes in cmip6. Geophysical Research Letters 49(11):e2021GL097511. https://doi.org/https://doi.org/10.1029/2021GL097511, URL https://agupubs.onlinelibrary.wiley.com/doi/abs/10.1029/2021GL097511, e2021GL097511 2021GL097511,

https://agupubs.onlinelibrary.wiley.com/doi/pdf/10.1029/2021GL097511

McKenna CM, Maycock AC (2021) Sources of uncertainty in multimodel large ensemble projections of the winter north atlantic oscillation. Geophysical Research Letters 48(14):e2021GL093258. https://doi.org/https://doi.org/10.1029/2021GL093258, URL https://agupubs.onlinelibrary.wiley.com/doi/abs/10.1029/2021GL093258, e2021GL093258 2021GL093258, https://agupubs.onlinelibrary.wiley.com/doi/pdf/10.1029/2021GL093258

Michel C, Li C, Simpson IR, et al (2020) The change in the enso teleconnection under a low global warming scenario and the uncertainty due to internal variability. Journal of Climate 33(11):4871 – 4889. https://doi.org/10.1175/JCLI-D-19-0730.1, URL https://journals.ametsoc.org/view/journals/clim/33/11/jcli-d-19-0730.1.xml

Newman M, Alexander MA, Ault TR, et al (2016) The pacific decadal oscillation, revisited. Journal of Climate 29(12):4399 – 4427. https://doi.org/10.1175/JCLI-D-15-0508.1, URL https://journals.ametsoc.org/view/journals/clim/29/12/jcli-d-15-0508.1.xml

O'Brien JP, Deser C (2023) Quantifying and understanding forced changes to unforced modes of atmospheric circulation variability over the north pacific in a coupled model large ensemble. Journal of Climate 36(1):19 – 37. https://doi.org/10.1175/JCLI-D-22-0101.1, URL https://journals.ametsoc.org/view/journals/clim/36/1/JCLI-D-22-0101.1.xml

Planton YY, Guilyardi E, Wittenberg AT, et al (2021) Evaluating Climate Models with the CLIVAR 2020 ENSO Metrics Package. Bulletin of the American Meteorological Society 102(2):E193 – E217. https://doi.org/10.1175/BAMS-D-19-0337.1, URL https://journals.ametsoc.org/view/journals/bams/102/2/BAMS-D-19-0337.1.xml

Planton YY, Lee J, Wittenberg AT, et al (2024) Estimating uncertainty in simulated enso statistics. Journal of Advances in Modeling Earth Systems 16(9):e2023MS004147. https://doi.org/https://doi.org/10.1029/2023MS004147, URL https://agupubs.onlinelibrary.wiley.com/doi/abs/10.1029/2023MS004147, e2023MS004147 2023MS004147, https://agupubs.onlinelibrary.wiley.com/doi/pdf/10.1029/2023MS004147

Power S, Delage F, Chung C, et al (2013) Robust twenty-first-century projections of elniño and related precipitation variability. Nature 502(7472):541–545. https://doi.org/10.1038/nature12580, URL https://doi.org/10.1038/nature12580

Risbey JS, Pook MJ, McIntosh PC, et al (2009) On the remote drivers of rainfall variability in australia. Monthly Weather Review 137(10):3233 – 3253. https://doi.org/10.1175/2009MWR2861.1, URL https://journals.ametsoc.org/view/journals/mwre/137/10/2009mwr2861.1.xml

Rodgers KB, Lee SS, Rosenbloom N, et al (2021) Ubiquity of human-induced changes in climate variability. Earth System Dynamics 12(4):1393–1411. https://doi.org/10.5194/esd-12-1393-2021, URL https://esd.copernicus.org/articles/12/1393/2021/

Shepherd TG (2014) Atmospheric circulation as a source of uncertainty in climate change projections. Nature Geoscience 7(10):703–708. URL https://doi.org/10.1038/ngeo2253

Simpson IR, Shaw TA, Ceppi P, et al (2025) Confronting earth system model trends with observations. Science Advances 11(11):eadt8035. https://doi.org/10.1126/sciadv.adt8035, URL https://www.science.org/doi/abs/10.1126/sciadv.adt8035, https://www.science.org/doi/pdf/10.1126/sciadv.adt8035

Smith DM, Dunstone NJ, Eade R, et al (2025) Mitigation needed to avoid unprecedented multi-decadal north atlantic oscillation magnitude. Nature Climate Change 15(4):403–410. URL https://doi.org/10.1038/s41558-025-02277-2

Suarez-Gutierrez L, Milinski S, Maher N (2021) Exploiting large ensembles for a better yet simpler climate model evaluation. Climate Dynamics 57(9):2557–2580. URL https://doi.org/10.1007/s00382-021-05821-w

Swart NC, Cole JNS, Kharin VV, et al (2019) The Canadian Earth System Model version 5 (CanESM5.0.3). Geoscientific Model Development 12(11):4823–4873. https://doi.org/10.5194/gmd-12-4823-2019, URL https://gmd.copernicus.org/articles/12/4823/2019/

Takahashi K, Montecinos A, Goubanova K, et al (2011) Enso regimes: Reinterpreting the canonical and modoki el niño. Geophysical Research Letters 38(10). https://doi.org/https://doi.org/10.1029/2011GL047364, URL https://agupubs.onlinelibrary.wiley.com/doi/abs/10.1029/2011GL047364, https://agupubs.onlinelibrary.wiley.com/doi/pdf/10.1029/2011GL047364

Tatebe H, Ogura T, Nitta T, et al (2019) Description and basic evaluation of simulated mean state, internal variability, and climate sensitivity in MIROC6. Geoscientific Model Development 12(7):2727–2765. https://doi.org/10.5194/gmd-12-2727-2019, URL https://gmd.copernicus.org/articles/12/2727/2019/

Visbeck MH, Hurrell JW, Polvani L, et al (2001) The north atlantic oscillation: Past, present, and future. Proceedings of the National Academy of Sciences 98(23):12876–12877. https://doi.org/10.1073/pnas.231391598, URL https://www.pnas.org/doi/abs/10.1073/pnas.231391598, https://www.pnas.org/doi/pdf/10.1073/pnas.231391598

Wallace JM, Gutzler DS (1981) Teleconnections in the geopotential height field during the northern hemisphere winter. Monthly Weather Review 109(4):784 – 812. https://doi.org/10.1175/1520-0493(1981)109⟨0784:TITGHF⟩2.0.CO;2, URL https://journals.ametsoc.org/view/journals/mwre/109/4/1520-0493_

1981_109_0784_titghf_2_0_co_2.xml

Wengel C, Lee SS, Stuecker MF, et al (2021) Future high-resolution el niño/southern oscillation dynamics. Nature Climate Change 11(9):758–765. https://doi.org/10.1038/s41558-021-01132-4, URL https://doi.org/10.1038/s41558-021-01132-4

van der Wiel K, Bintanja R (2021) Contribution of climatic changes in mean and variability to monthly temperature and precipitation extremes. Communications Earth & Environment 2(1):1. URL https://doi.org/10.1038/s43247-020-00077-4

Yuan J, Tan B, Feldstein SB, et al (2015) Wintertime north pacific teleconnection patterns: Seasonal and interannual variability. Journal of Climate 28(20):8247 – 8263. https://doi.org/10.1175/JCLI-D-14-00749.1, URL https://journals.ametsoc.org/view/journals/clim/28/20/jcli-d-14-00749.1.xml

Zhou ZQ, Xie SP, Zheng XT, et al (2014) Global warming–induced changes in el niño teleconnections over the north pacific and north america. Journal of Climate 27(24):9050 – 9064. https://doi.org/10.1175/JCLI-D-14-00254.1, URL https://journals.ametsoc.org/view/journals/clim/27/24/jcli-d-14-00254.1.xml

Ziehn T, Chamberlain MA, Law RM, et al (2020) The Australian Earth System Model: ACCESS-ESM1.5. JSHESS 70(1):193–214. URL https://doi.org/10.1071/ES19035

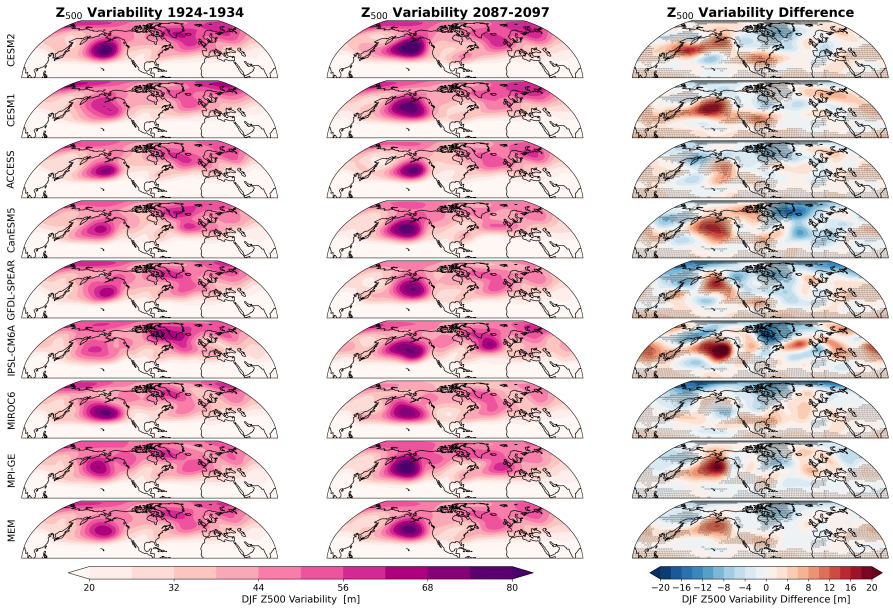


Fig. 1 Projected change in 500hPa geopotential height (Z500) variability across SMILEs. Z500 variability is calculated as a standard deviation across the ensemble for (left) the early period (1924-1934), (middle) the late period (2087-2097), and (right) their difference (late minus early) for each SMILE and the multi-ensemble mean (MEM). Stippling in the right column shows where at least 7 SMILEs agree on the sign of the projected change. The variability in each decade is based on individual DJF seasons, not decadal averages, and the MEM results are based on computing the mean standard deviation by taking the square-root of the mean variance across models.

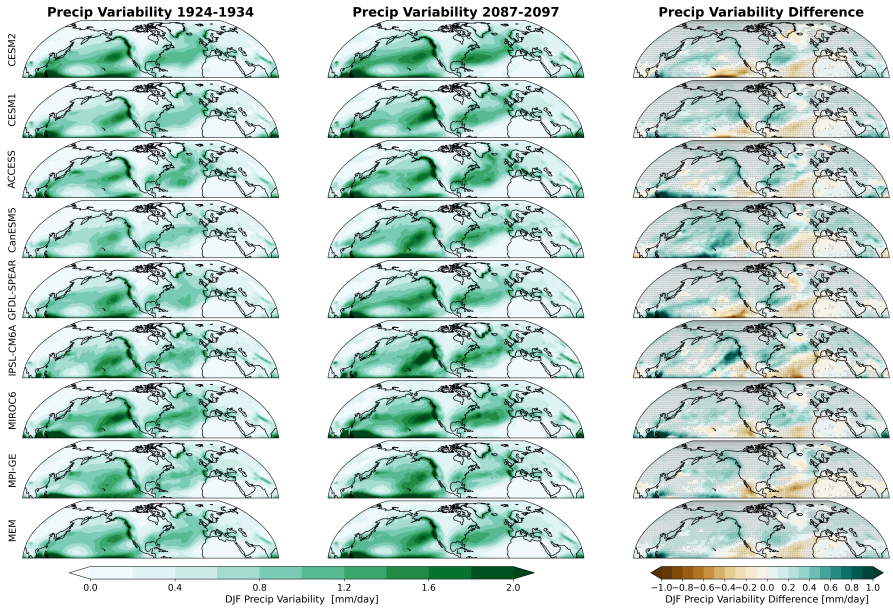


Fig. 2 Projected change in precipitation variability across SMILEs. As in Figure 1 except for precipitation variability.

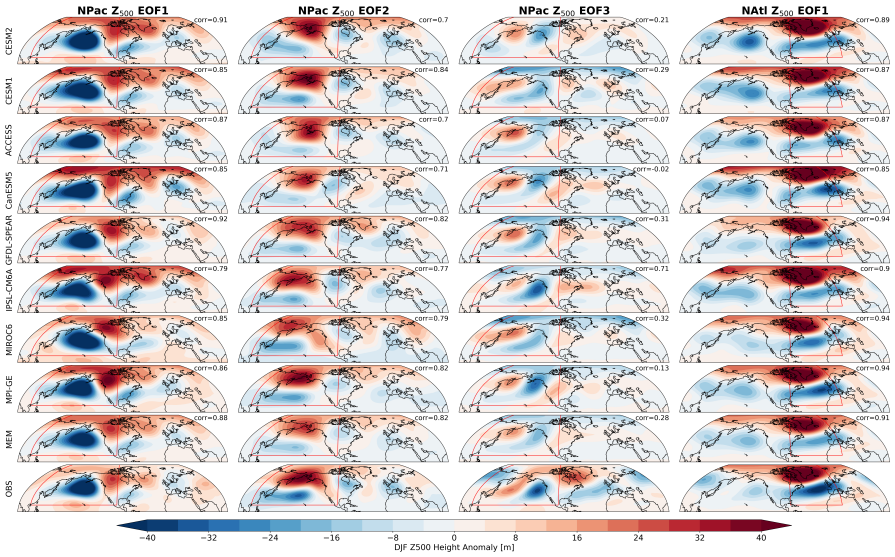


Fig. 3 Traditional (time-based) EOFs of Z500 variability over the North Pacific and Atlantic for the historical period (1950-2015) for the 8 SMILEs, the multi-ensemble mean (MEM, computed as the average of the eight SMILE regression maps) and observations from NOAA/CIRES/DOE 20th Century Reanalysis (V3). Observations are detrended by removing a quadratically fitted polynomial from each grid point, while the SMILEs are detrended by removing the ensemble mean. The pattern correlation of each map with the observed map for the domains where the EOFs are computed (illustrated using the red box) is shown in the top right corner of each subplot. The EOFs for tropical Pacific SST variability are shown in Figure S1. SEOFs for the same period are shown in Figure S2 for comparison. Note that NPac Z500 EOF1,2,3 are the PNA, NPO and EPP respectively, and NAtl Z500 EOF 1 is the NAO.

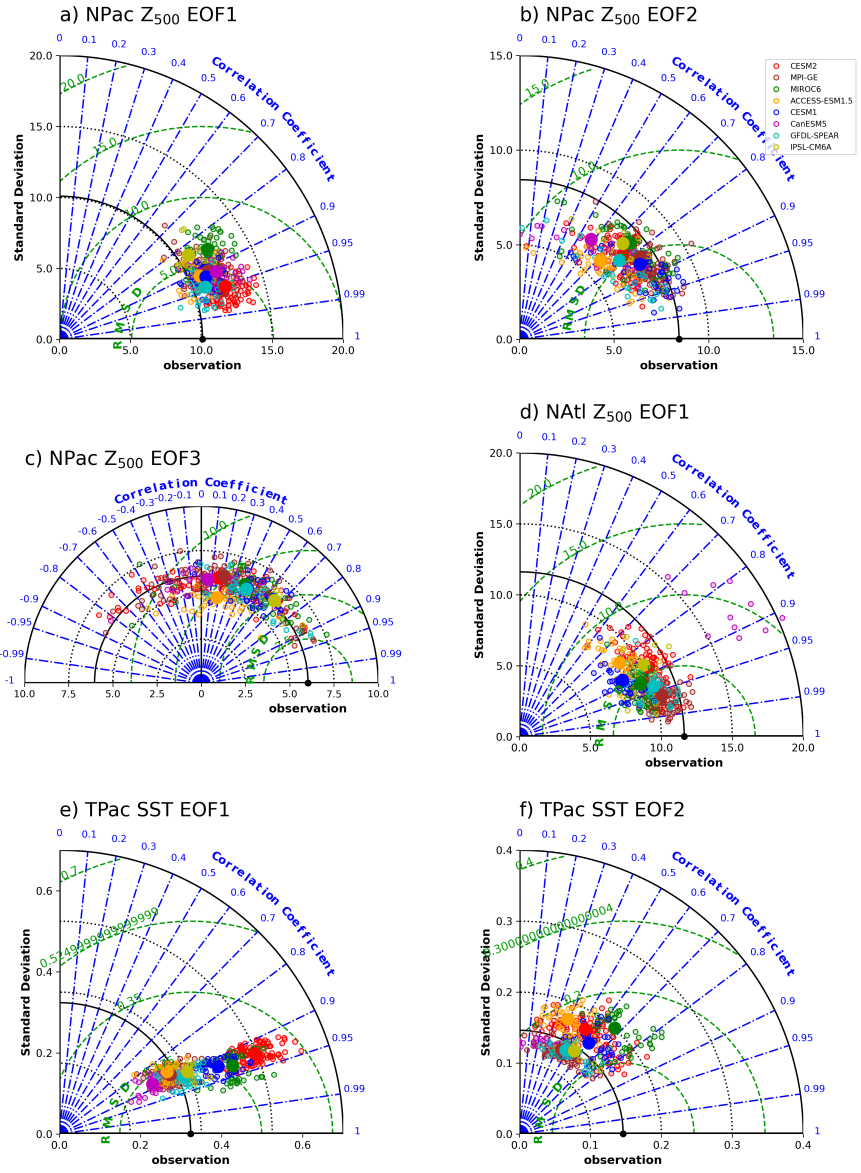


Fig. 4 Taylor diagram for each SMILE EOF compared to observations. Shown for North Pacific Z500 EOFs 1-3, North Atlantic Z500 EOF1 and Tropical Pacific SST EOFs 1-2. The Taylor diagram shows each SMILE in a different colour with the small dots individual ensemble members and the large dot the ensemble mean. Observations are shown in black. Z500 observations are from NOAA/CIRES/DOE 20th Century Reanalysis (V3) (1950-2015) and SST observations are from ERSSTv5 (1950-2015) (Huang et al, 2017). For this plot the EOFs are computed against time for the same period as the observations for each ensemble member. The plot shows the pattern correlation with observations in blue lines, the root mean squared difference (RMSD) in green circles and the standard deviation in black. Higher correlations, lower RMSD and a standard deviation close to the black observational dot indicate that the model is closer to observations. For this analysis the forced response is removed from the SMILE by removing the ensemble mean at each timestep. The observations are detrended using a quadratic fit. We note that detrending the SMILEs by removing a quadratic fit gives a qualitatively similar answer (not shown). The EOF patterns for both observations and SMILEs used in this Figure are shown in Figure S3. Note that NPac Z500 EOF1,2,3 are the PNA, NPO and EPP respectively, NAtl Z500 EOF 1 is the NAO, and TPac SST EOF1,2 are the first and second components of ENSO.

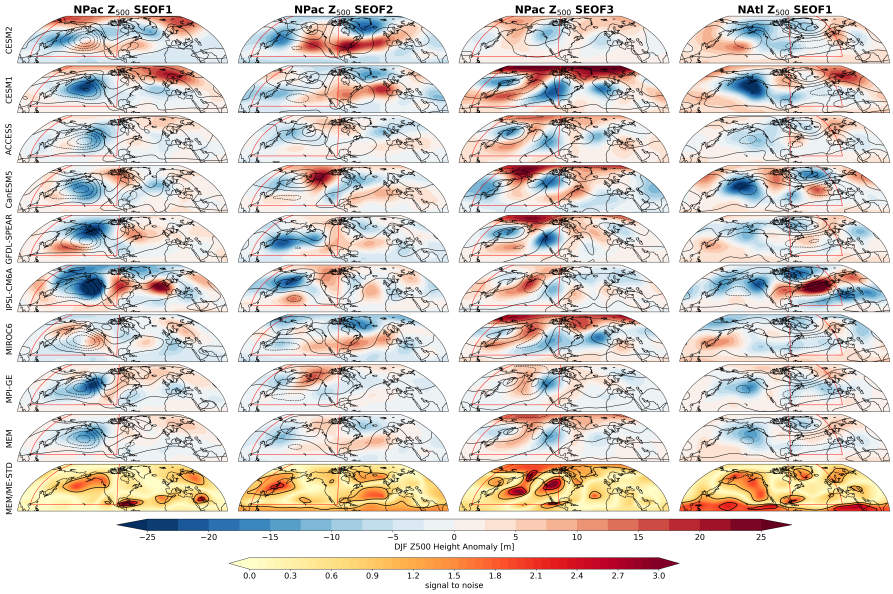


Fig. 5 Projected change in the North Pacific and North Atlantic Z500 SEOFs regressed back onto Z500. Each SEOF is regressed onto Z500 in DJF. Shown is the change in this regression in 2087-2097 compared to 1924-1934. Shown for each SMILE, the multi-ensemble mean (MEM) and the signal-to-noise ratio defined as the MEM divided by the standard deviation across the 8 SMILE means (ME-STD). Contours show the baseline period 1924-1934 for reference (range of -90 to 90m). Contours on the signal-to-noise ratio show the values 1 and 2. Full projection for the later period is shown in Figure S4. Note that NPac Z500 EOF1,2,3 are the PNA, NPO and EPP respectively, and NAtl Z500 EOF 1 is the NAO.

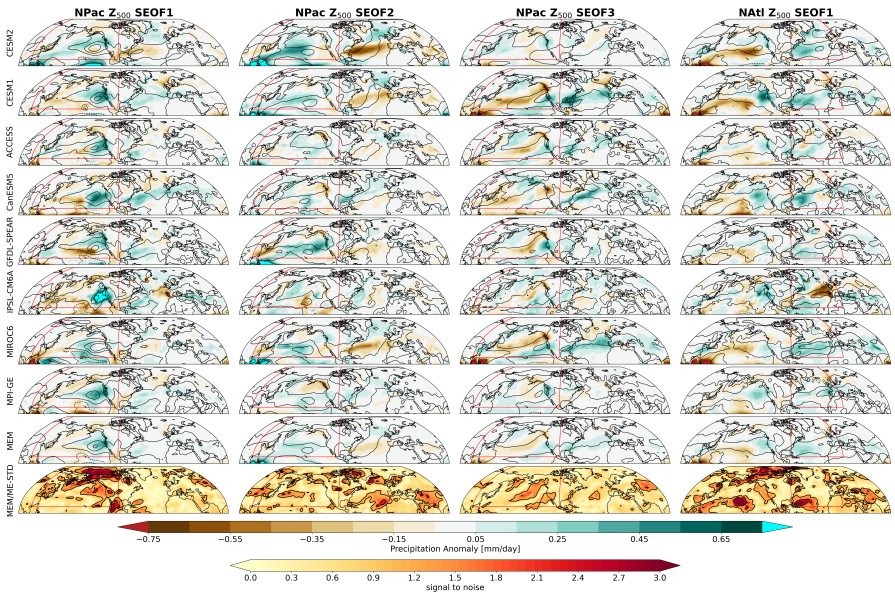


Fig. 6 Projected change in the North Pacific and North Atlantic Z500 SEOFs regressed onto precipitation. As in Figure 5 except for precipitation. Full projection for the later period is shown in Figure S5. Note that the precipitation reference contours are based on a range of -1 to 1mm/day. Note that NPac Z500 EOF1,2,3 are the PNA, NPO and EPP respectively, and NAtl Z500 EOF 1 is the NAO.

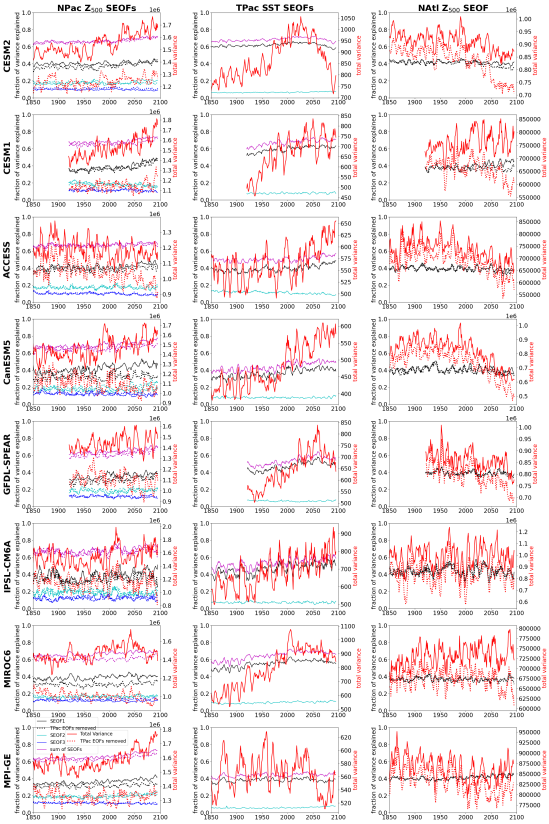


Fig. 7 Variance explained by each SEOF and total variance in each region. Variance explained for each SEOF is shown for each of the 8 SMILES. The total variance is shown in red. For the North Pacific and North Atlantic SEOFs the dotted lines indicate the total variance and variance explained when the influence of the two tropical Pacific SEOFs are removed. Variance units are the square of the original units of the data. Note that NPac Z500 EOF1,2,3 are the PNA, NPO and EPP respectively, NAtl Z500 EOF 1 is the NAO, and TPac SST EOF1,2 are the first and second components of ENSO.

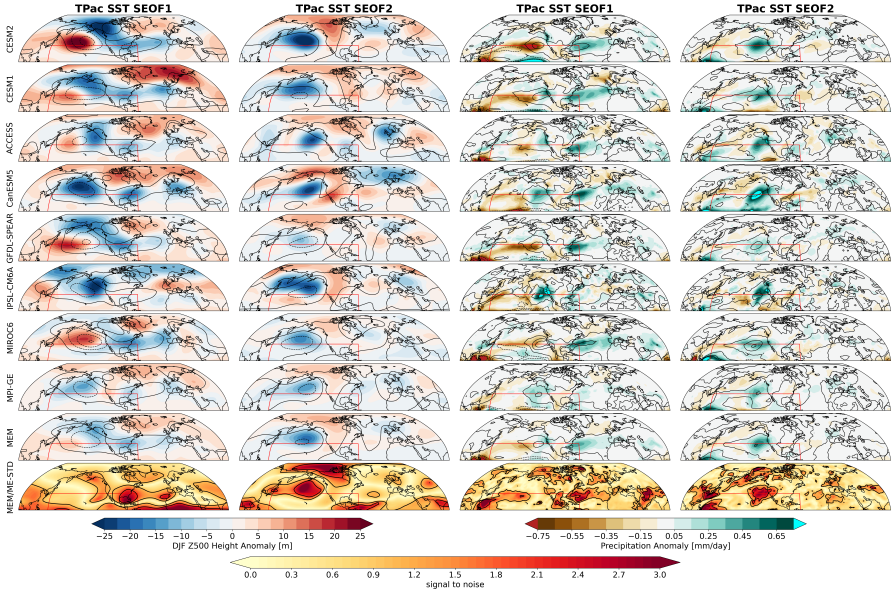


Fig. 8 Projected change in the Tropical Pacific SST SEOFs regressed onto Z500 and precipitation. Each SEOF is regressed onto Z500 (left) and precipitation (right) in DJF. Shown is the change in this regression in 2087-2097 compared to 1924-1934. Shown for each SMILE, the multi-ensemble mean (MEM) the signal-to-noise ratio defined as the MEM divided by the standard deviation across the 8 SMILE means (ME-STD). Contours show the baseline period 1924-1934 for reference. Contours on the signal-to-noise ratio show the values 1 and 2. Full projections are shown in Figure S6 and S7. Note that TPac SST EOF1,2 are the first and second components of ENSO.

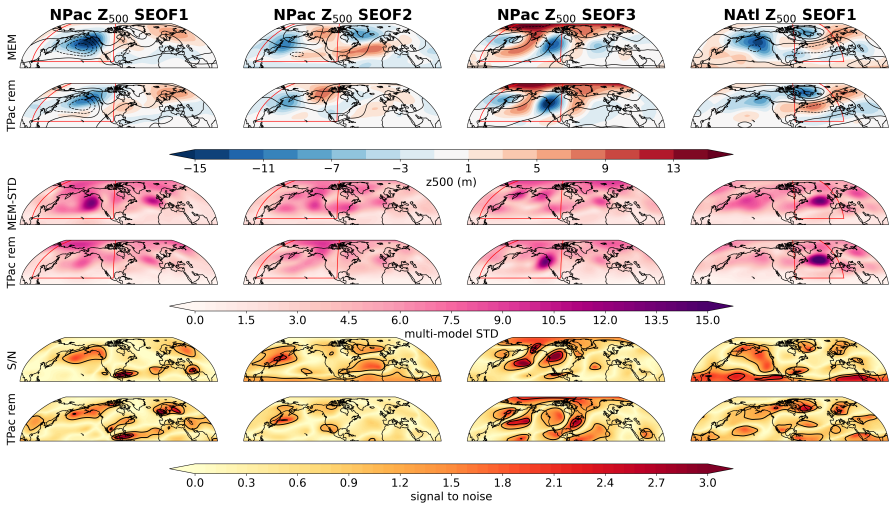


Fig. 9 Summary of influence of removing the tropical Pacific SEOFs on Z500. Each SEOF is regressed onto Z500 in DJF. Shown is the change in this regression in 2087-2097 compared to 1924-1934. The top two row show the multi-ensemble mean (MEM) of this change (first row) and the change once the influence of the tropical Pacific is removed (second row). Contours show the baseline period 1924-1934 for reference. The multi-ensemble STD (ME-STD) of the change is shown in the second two rows (first row) and ME-STD once the influence of the topical Pacific is removed (second row). The bottom two rows show the signal-to-noise ratio of the change defined as the MEM divided by the standard deviation across the 8 SMILE means (ME-STD) (first row) and once the influence of the tropical Pacific is removed (second row). Contours on the signal-to-noise ratio show the values 1 and 2. Individual models are shown in Figure S10. Note that NPac Z500 EOF1,2,3 are the PNA, NPO and EPP respectively, and NAtl Z500 EOF 1 is the NAO.

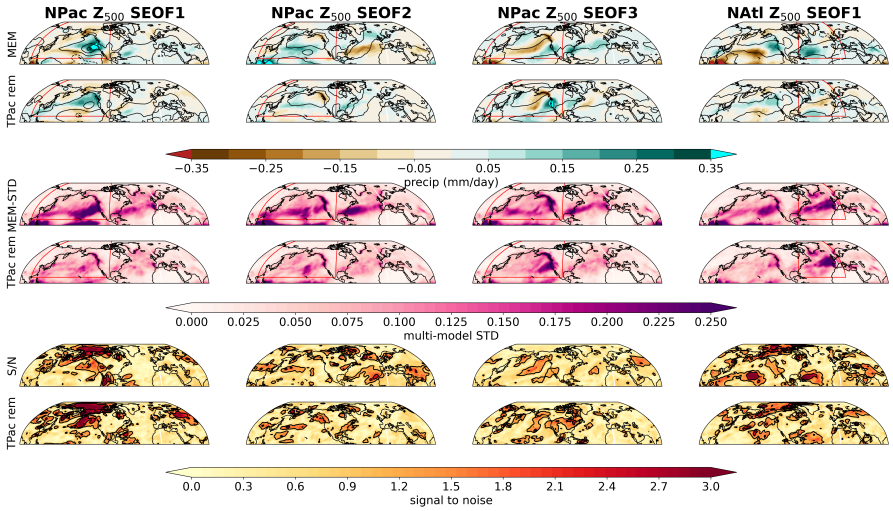


Fig. 10 Summary of influence of removing the tropical Pacific SEOFs on precipitation. Same as Figure 9 except for precipiation. Individual models are shown in Figure S11. Note that NPac Z500 EOF1,2,3 are the PNA, NPO and EPP respectively, and NAtl Z500 EOF 1 is the NAO.

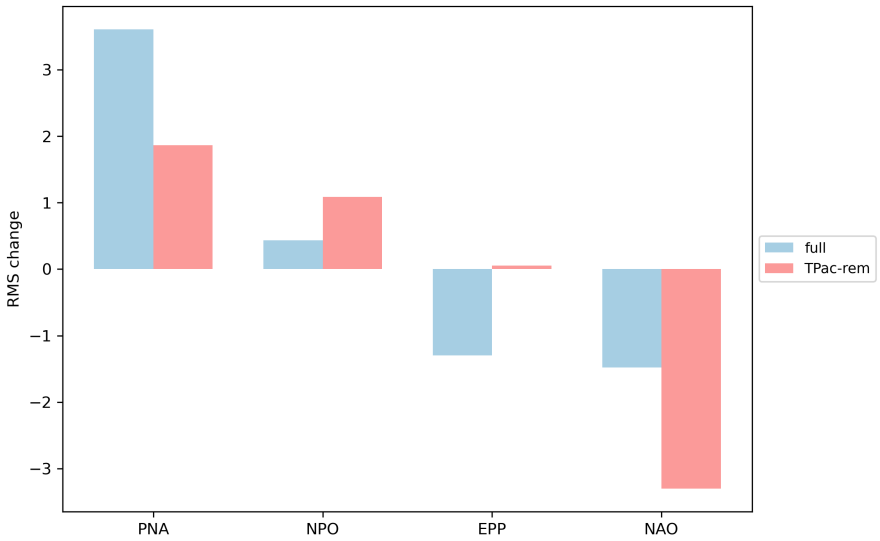


Fig. 11 Change in RMS of the ensemble mean projected change in North Pacific and North Atlantic Z500 SEOFs regressed back onto Z500 for each region itself. Shown for the full projection (blue) and with the tropical Pacific influence regressed out (pink). The change is computed as the RMS in 2087 - 2097 minus the RMS in 1924-1934 over the individual regions that the SEOFs are computed in.

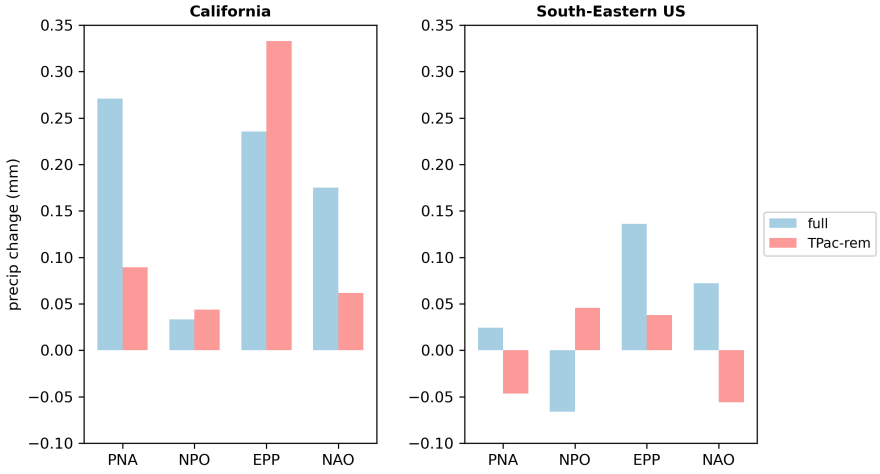


Fig. 12 Californian and South-Eastern US precipitation variability related to each mode and after removing the influence of the leading two modes of tropical Pacific SST variability. Mean precipitation at each timestep over California (left; 234-245E, 31-44N) and the South-Eastern US (right; 270-286E, 24-36N) calculated as a regression of precipitation onto each Z500 mode in each SMILE before (blue) and after (pink) removing the influence of the two leading modes of tropical Pacific SST variability.